



Frugal random exploration strategy for shape recognition using statistical geometry

Samuel Hidalgo-Caballero ^{1,2}, Alvaro Cassinelli,³ Emmanuel Fort,² and Matthieu Labousse ^{1,*}

¹*Gulliver, CNRS, ESPCI Paris, Université PSL, 75005 Paris, France, European Union*

²*Institut Langevin, ESPCI Paris, Université PSL, CNRS, 75005 Paris, France, European Union*

³*School of Creative Media City, City University of Hong Kong, 18 Tat Hong Ave, Kowloon Tong, Hong Kong*



(Received 9 January 2024; accepted 20 March 2024; published 26 April 2024)

Very distinct strategies can be deployed to recognize and characterize an unknown environment or a shape. A recent and promising approach, especially in robotics, is to reduce the complexity of the exploratory units to a minimum. Here, we show that this frugal strategy can be taken to the extreme by exploiting the power of statistical geometry and introducing different invariant features. We show that an elementary robot devoid of any orientation or location system, exploring randomly, can access global information about an environment such as the values of the explored area and perimeter. The explored shapes are of arbitrary geometry and may even nonconnected. From a dictionary, this most simple robot can thus identify various shapes such as famous monuments and even read a text.

DOI: [10.1103/PhysRevResearch.6.023103](https://doi.org/10.1103/PhysRevResearch.6.023103)

I. INTRODUCTION

Image, object, or environment recognition is a highly complex operation which involves acquiring a global information based on spatial correlations. The standard strategy is centralized using multiplexed sensors coupled to complex computational capacities and data processing which can be possibly implemented in high-tech robotic systems. Recently, an alternative fruitful strategy has emerged based on the simple cost-effective basic units collecting unsupervised information, no direct localization capacities, and eventually working in parallel in an unmanned manner [1,2]. This strategy is more robust and well-suited for analysis and exploration with restricted computational and hardware resources, and in the case of harsh or complex environments for which part of the information is not accessible. The most elementary system one can imagine is limited to the acquisition of a local information only with no possible communication, localization capacity, or orientation awareness.

The unavailability of localization capability and the associated randomness of the exploration make the use of statistical geometry crucial to move from local information to a global knowledge of the environment. In this context, the statistical properties of chord length are distributed across various kinds of geometrical shapes. A chord length is defined as the Euclidean distance of a segment linking two points at the boundary of a given two-dimensional domain. Only segments which are fully included in the domain are classified as a chord. The distribution of these chord lengths plays a central role for the characterization of size and shape of the intercepted

objects with applications such as in acoustics, ecology [3–6], image analysis [7,8], stereology [9–11], and reactor design [12–15]. The moments of the chord length distributions are related to mathematical invariants and give access to global geometrical parameters such as the volume, the surface, or the perimeter of objects. As a historical example, the Cauchy formula states that the mean chord length is proportional to the ratio of the volume of an object to its surface area for a three-dimensional (3D) object, or to the ratio of its area to its perimeter for a 2D object [16,17]. Recent generalization to random motion [18–23], to closed trajectories [24,25], and to wave propagation properties [26–28] have renewed interest for such invariants. Unfortunately, most of theorems of this field of mathematics are restricted to convex shapes and with no inclusions which limit the statistical approach for exploration and pattern recognition.

Here, we introduce statistical invariants that extend to any arbitrary, possibly nonconvex, nonconnected or with inclusions shapes. This generalization allows us to revisit and push the limits of frugal exploration strategies to its most minimalistic version by fully integrating the assets of statistical geometry. We show experimentally that an elementary robot devoid of any localization, orientation, and observation systems can assess the surface and perimeter of a two-dimensional region in which it evolves with random displacements. Then, with the help of a dictionary, we show how it recognizes these shapes. We also discuss the benefits of global over sequential exploration strategies in the case of nonconnected shapes and apply it to reading strategies.

II. RESULTS

A. Generalized statistical geometry invariants

Statistical geometry establishes a link between probabilities arising from local properties and global geometric quantities. Cauchy's theorem plays a central role in relating the average chord length of a random distribution $\langle \ell \rangle_{\text{chords}}$

*Corresponding author: matthieu.Labousse@espci.fr

Published by the American Physical Society under the terms of the [Creative Commons Attribution 4.0 International license](https://creativecommons.org/licenses/by/4.0/). Further distribution of this work must maintain attribution to the author(s) and the published article's title, journal citation, and DOI.

to the ratio of the area A to the perimeter P of the explored domain. The average is realized over all possible chords of the domain. In two dimensions, it reads $\langle \ell \rangle_{\text{chords}} = \pi A/P$. The Crofton-Hostinsky theorem [17] uses the third moment, and in two dimensions satisfies $\langle \ell^3 \rangle_{\text{chords}} = 3A^2/P$ so that combining these two theorems can yield P and A separately which could provide a frugal and powerful recognition strategy. While Cauchy's theorem can be extended to nonconvex shapes [29] unfortunately, the Crofton-Hostinsky theorem is only valid for convex shapes, which in practice, prohibits its relevance for exploration and pattern recognition purposes. A generalization of this theorem to arbitrary forms is therefore essential. To this end, we introduce an alternative statistical invariant. We first label the intersections between a straight trajectory L and the boundaries of the explored shape according to whether they are ingoing i or outgoing o from the shape. We then derive all the distances between pairs of intersections by distinguishing the chords depending on their ends: l_{io} , l_{ii} , or l_{oo} . We define the geometric function of order $n \in \mathbb{N}$ associated to the line L , $\mathcal{L}_n(L) = \sum_{i,o} \ell_{io}^n - \sum_o \ell_{oo}^n - \sum_i \ell_{ii}^n$. Following a mathematical demonstration detailed in the following section, we find that the area of the explored shape A satisfies

$$A = \frac{\pi \langle \mathcal{L}_3 \rangle_{\text{lines}}}{3 \langle \mathcal{L}_1 \rangle_{\text{lines}}} \quad (1)$$

with the average being made with respect to all straight lines crossing the shapes. This relation, combined with Cauchy's theorem, allows statistical geometry to be used for exploration and pattern recognition by measuring P and A independently. It applies to any arbitrary shape, whether nonconvex, with inclusions, and even nonconnected. This establishes an autonomous strategy for obtaining global geometric features without any *a priori* assumptions.

B. Demonstration of Eq. (1)

Before implementing this strategy in real-world conditions, we demonstrate Eq. (1). First, let us consider the case of a simple nonconvex domain Ω with border $\partial\Omega$, surface area A , and perimeter P , as depicted in Fig. 1(a). We assume that the domain Ω must have a measurable area A and a measurable perimeter P .

We consider a line L intersecting the border $\partial\Omega$. A point belonging to the line L is identified by its curvilinear abscissa l along the line. For every line, we enumerate the points where the line enters and exits the domain. With \mathcal{N} being the number of chords belonging to a given line L , we denote by $(i_k)_{k=1, \dots, \mathcal{N}}$ the curvilinear abscissa of the entries and by $(o_k)_{k=1, \dots, \mathcal{N}}$ the curvilinear abscissa of the exits. For a convex body, we have $\mathcal{N} = 1$ for all the possible lines intersecting $\partial\Omega$. For the shape shown in Fig. 1(a), $\mathcal{N} = 1, 2$, etc. The number of lines is quantified by using the kinematic measure $dL = d\rho d\theta$, where (ρ, θ) denotes the usual radial coordinates, with an origin placed inside the domain Ω [17]. Let us consider two points P_1 with abscissa l_1 and P_2 with abscissa l_2 inside the domain and belonging to a given line L . We denote $r = |l_2 - l_1|$ as the distance between P_1 and P_2 . For any given integer n we consider the integral

$$J_n = \int_{(P_1, P_2) \in \Omega \times \Omega} r^n d^2P_1 d^2P_2. \quad (2)$$

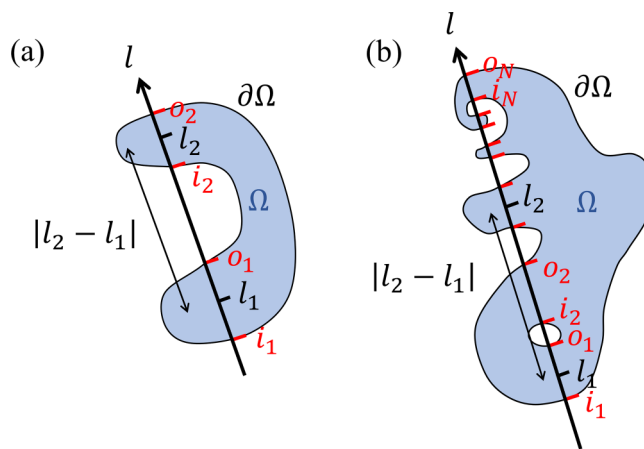


FIG. 1. (a) Simple and (b) complex nonconvex domain Ω intersected by a nonoriented line L . Two points P_1 with curvilinear abscissa l_1 and P_2 with abscissa l_2 inside the domain belonging to a line L are plotted. This line has (a) two entries in (i_1, i_2) and two exits (o_1, o_2) or (b) \mathcal{N} entries in $(i_1, \dots, i_{\mathcal{N}})$ and \mathcal{N} exits in $(o_1, \dots, o_{\mathcal{N}})$.

Note that for $n = 0$, we have

$$J_0 = \int_{P_1 \in \Omega} d^2P_1 \times \int_{P_2 \in \Omega} d^2P_2 = A^2. \quad (3)$$

Then let us call f the characteristic function such that $f(P) = 1$ if $P \in \Omega$ and $f(P) = 0$ otherwise. Finally, the terms $d^2P_1 d^2P_2$ can be expressed in the system of the line coordinates with the Jacobian given in [17], $d^2P_1 d^2P_2 = |l_2 - l_1| dl_1 dl_2 dL$. It gives

$$J_n = \int f(P_1) f(P_2) |l_2 - l_1|^{n+1} dl_1 dl_2 dL. \quad (4)$$

The integration on dL is realized over every possible line L intersecting the external border $\partial\Omega$ while the integrations on dl_1 and dl_2 are such that P_1 and P_2 remain in Ω . It gives

$$J_n = \int_{L: L \cap \partial\Omega \neq \emptyset} dL \int dl_1 f(P_1) \int dl_2 f(P_2) |l_2 - l_1|^{n+1}. \quad (5)$$

We separate the sets of lines L into two sets L_1 and L_2 . A line in L_1 enters once in the domain at a point i_1 and exits once at a point o_1 . A line of L_2 has two entries (i_1, i_2) and two exits (o_1, o_2) in the domain Ω as exemplified in Fig. 1(a). It yields

$$J_n = \sum_{j=1}^2 \int_{L_j: L_j \cap \partial\Omega \neq \emptyset} dL_j \int dl_1 f(P_1) \int dl_2 f(P_2) |l_2 - l_1|^{n+1}, \quad (6)$$

which we can write in the compact form

$$J_n = \sum_{j=1}^2 J_n^{(j)}. \quad (7)$$

The computation of $J_n^{(1)}$ gives us

$$J_n^{(1)} = \frac{2}{(n+2)(n+3)} \int_{L_1: L_1 \cap \partial\Omega \neq \emptyset} dL_1 (o_1 - i_1)^{n+3}, \quad (8)$$

which is the same result as for convex shapes [17]. For a line L_2 , the point P_1 can be either in or out of the domain Ω by sliding along the line L_2 . It means that l_1 must be integrated along two intervals $[i_1, o_1]$ and $[i_2, o_2]$ corresponding to P_1 being in Ω . The integrals can be performed explicitly, which yields

$$J_n^{(2)} = \frac{2}{(n+2)(n+3)} \int_{L_2: L_2 \cap \partial\Omega \neq \emptyset} dL_2 [(o_2 - i_1)^{n+3} + (o_1 - i_1)^{n+3} + (o_2 - i_2)^{n+3} + (i_2 - o_1)^{n+3}] - [(o_2 - o_1)^{n+3} - (i_2 - i_1)^{n+3}]. \tag{9}$$

By combining Eqs. (7), (8), and (9) for $n = 0$, with Eq. (2) we get

$$A^2 = \frac{1}{3} \int_{L_1: L_1 \cap \partial\Omega \neq \emptyset} dL_1 (o_1 - i_1)^3 + \frac{1}{3} \int_{L_2: L_2 \cap \partial\Omega \neq \emptyset} dL_2 [(o_2 - i_1)^3 + (o_1 - i_1)^3 + (o_2 - i_2)^3 + (i_2 - o_1)^3] - [(o_2 - o_1)^3 + (i_2 - i_1)^3], \tag{10}$$

or equivalently and in a more compact form

$$A^2 = \frac{1}{3} \int_{L: L \cap \partial\Omega \neq \emptyset} dL \mathcal{L}_3(L). \tag{11}$$

We now want to evaluate $\langle \mathcal{L}_3(L) \rangle_{\text{lines}}$, the mean value of $\mathcal{L}_3(L)$ among all possible lines L uniformly, isotopically distributed, and intersecting $\partial\Omega$. The probability $p(L)dL$ to measure a line L intersecting $\partial\Omega$ is

$$p(L)dL = \frac{dL}{\int_{L: L \cap \partial\Omega \neq \emptyset} dL}. \tag{12}$$

So, the mean value $\langle \mathcal{L}_3(L) \rangle_{\text{lines}}$ over all possible lines intersecting $\partial\Omega$ can be computed by

$$\langle \mathcal{L}_3(L) \rangle_{\text{lines}} = \int_{L: L \cap \partial\Omega \neq \emptyset} \mathcal{L}_3(L) p(L) dL = \frac{\int_{L: L \cap \partial\Omega \neq \emptyset} \mathcal{L}_3(L) dL}{\int_{L: L \cap \partial\Omega \neq \emptyset} dL} = \frac{3A^2}{\int_{L: L \cap \partial\Omega \neq \emptyset} dL}. \tag{13}$$

The generalization for more complex nonconvex domains such as shown in Fig. 1(b) is obtained by considering Eq. (5) and by dividing the set of all lines intersecting $\partial\Omega$ into the sets $L_1, L_2, L_3, \dots, L_N$ having respectively 1, 2, 3, \dots, N exits and entries. The rest of the demonstration follows the same steps as above. As a result, we obtain the generalized version of the Crofton-Hostinský formula for nonconvex shapes in two dimensions:

$$\langle \mathcal{L}_3(L) \rangle_{\text{lines}} = \frac{3A^2}{\int_{L: L \cap \partial\Omega \neq \emptyset} dL}. \tag{14}$$

The last step of the demonstration considers the first moment to obtain an extended version of the Cauchy's mean chord theorem,

$$\begin{aligned} \mathcal{L}_1(L) &= \sum_{k,j} |o_k - i_j| - \sum_{k,j} |o_k - o_j| - \sum_{k,j} |i_k - i_j| \\ &= \sum_k |o_k - i_k|. \end{aligned} \tag{15}$$

Hence, $\mathcal{L}_1(L)$ represents the sum of lengths of all the chords belonging to the same line that cross the domain Ω . Its mean value of all possible lines intersecting $\partial\Omega$ yields [17,29]

$$\langle \mathcal{L}_1(L) \rangle_{\text{lines}} = \frac{\int_{L: L \cap \partial\Omega \neq \emptyset} \mathcal{L}_1(L) dL}{\int_{L: L \cap \partial\Omega \neq \emptyset} dL} = \frac{\pi A}{\int_{L: L \cap \partial\Omega \neq \emptyset} dL}. \tag{16}$$

Finally, by dividing Eq. (14) over Eq. (16), we obtain

$$\frac{\langle \mathcal{L}_3(L) \rangle_{\text{lines}}}{\langle \mathcal{L}_1(L) \rangle_{\text{lines}}} = \frac{3A}{\pi}, \tag{17}$$

and achieve our demonstration of Eq. (1) for any domain regardless of its topology.

C. Implementation with an elementary robot

We experimentally implement this frugal exploration strategy to evaluate the robustness of Eq. (1) under real conditions. We use a commercial toy robot called Sphero [30] which is a self-propelled rolling sphere [see Fig. 2(a)]. Sphero is a transparent spherical robot of 7 cm in diameter, with two encoded motors enabling a straight motion. The built-in battery can be recharged using an inductive charger. The robot speed can be programmed between 1 and 50 mm/s, with autonomy from 1 to 4 h. It features a 2-mm-diameter light sensor, a multicolor LED, an internal clock, and an accelerometer. It also has a Bluetooth connection with a range of 30 m to communicate with a computer or other devices. The robot can be programmed using blocks or JavaScript. The robot is enclosed in a closed arena in the shape of a rectangle of size $1.2 \times 1.5 \text{ m}^2$ and made of aluminum Norcan bars (square section, 2 in. wide) rigidly screwed together. The edges are detected by measuring an abrupt change of acceleration. The shape to recognize, such as the Eiffel Tower [Fig. 1(b)], is projected using a video projector placed above the arena explored by the robot.

The robot performs a series of uncorrelated straight linear motions at 10 mm/s, changing direction randomly as it detects the edge of the arena [Fig. 2(a); see Supplemental Material Movie 1 [31]]. Crucially, the robot possesses no information about either its absolute position or its direction. From the light received by the sensor, the robot can only detect if it

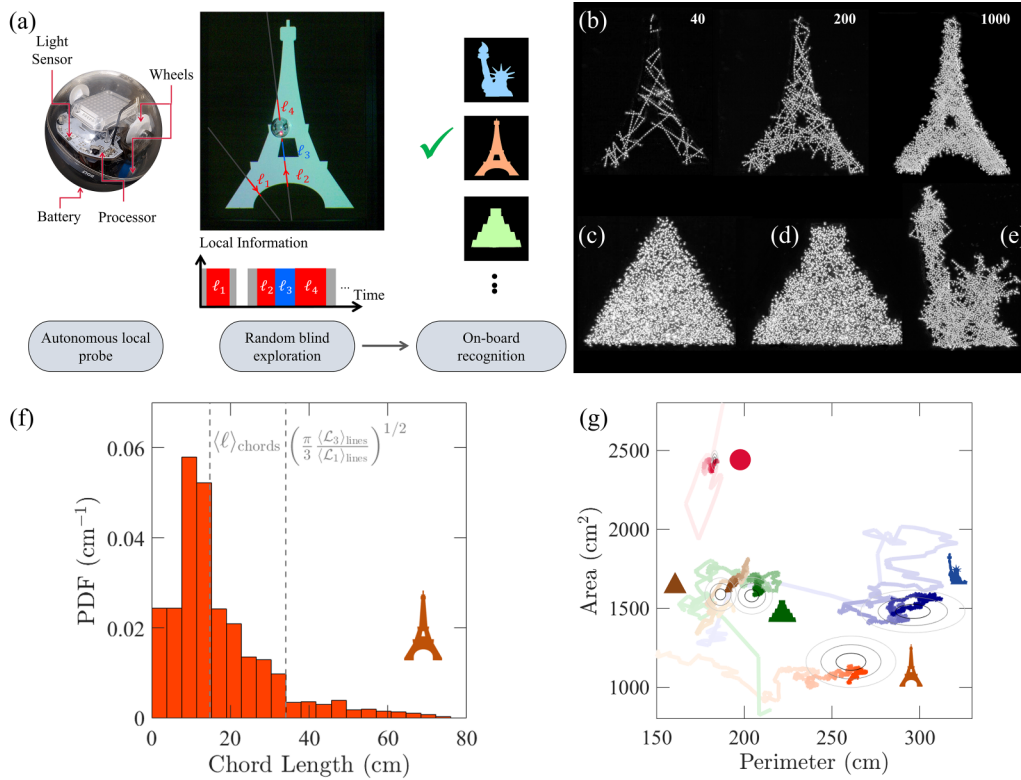


FIG. 2. Principle and implementation of robotic shape recognition by random exploration. (a) Photo and structure of the autonomous Sphero toy robot. (b)–(d) Exploration of a projected Eiffel Tower shape (b) by random straight-line motion acquiring only the chord lengths. Using statistical geometry to compute invariant quantities and shape parameters such as the perimeter P and the area A of the explored shape enables recognition from a dictionary. Snapshots of accumulated experimental light blinks emitted by the robot during its exploration of the Eiffel Tower for $N = 40$, 200, and 1000 lines (b) and for a triangle (c), the Chichen Itzá pyramid (d), and the Statue of Liberty for $N = 1000$ lines (e). (f) Chord length probability density function (PDF) for the Eiffel Tower shape with the mean chord length invariant $\langle \ell \rangle_{\text{chords}}$ and $A^{1/2} = \left(\frac{\pi \langle \mathcal{L}_3 \rangle_{\text{lines}}}{3 \langle \mathcal{L}_1 \rangle_{\text{lines}}} \right)^{1/2}$ for comparison. (g) Trajectories followed by the estimated parameters (P, A) as the number of lines N increases (increasing line contrast) in the perimeter-area representation space for various explored shapes. 75%, 95%, and 99% statistical confidence limits associated to each shape estimated by Monte Carlo simulations for $N = 1000$ (ellipses with increasing contrast and decreasing size).

is inside or outside the projected shape. From the times of entries and exits of the shape along the line L , the chord lengths are deduced and the functions $\mathcal{L}_1(L)$ and $\mathcal{L}_3(L)$ are calculated on board. From the statistical averages, the area A and the perimeter P of the projected shape are deduced from Eq. (1) and Cauchy's theorem. Note that the memory required to perform the calculations is limited, containing only the time of intersection events along the latest line to update the previously calculated mean values. Shape recognition is then performed using a dictionary containing a list of area and perimeter entries for a given shape, associated in the present case to famous monuments [Figs. 2(b)–2(e); see Supplemental Material Sec. 1 [31]]. Although two different objects can have the same entries, we found in practice that this was hardly ever the case, with up to hundreds of entries. Figure 2(b) shows the accumulated experimental trajectories during the robot exploring the Eiffel Tower for $N = 10, 100,$ and 1000 random trajectories. An external camera was used to follow the on-board LED which blinks when it is inside of the domain. The final exploration for the other shapes is shown in Figs. 2(c)–2(e) ($N = 1000$). The explorations

are found homogenous and statistically isotropic. The experimental chord distribution for the Eiffel Tower is shown in Fig. 2(f); its average value $\langle \ell \rangle_{\text{chords}}$ and $\frac{\pi \langle \mathcal{L}_3 \rangle_{\text{lines}}}{3 \langle \mathcal{L}_1 \rangle_{\text{lines}}}$ are geometrical invariant (while $\langle \mathcal{L}_1 \rangle_{\text{lines}}$ and $\langle \mathcal{L}_3 \rangle_{\text{lines}}$ are not). The trajectories followed by the estimated parameters and areas as the number of lines N increases (increasing line contrast) can be plotted in a {Perimeter-Area} representation space for various explored shapes [Fig. 2(g); see Supplemental Material Movie 2 [31]]. The statistical ellipses of confidence in the representation space {Perimeter-Area} are deduced from the confidence intervals of the area and the perimeter; these are estimated by Monte Carlo simulations consisting in generating of 10^3 independent runs, each of them consisting in generating $N = 1000$ independent lines. The increasingly small ellipses in Fig. 2(g) show the 75%, 95%, and 99% confidence ellipses associated to each shape. This proves that the robots discriminate each registered shape in the dictionary without any statistical ambiguity even though some shapes are very similar, such as in the case of the triangle and the Chichen Itzá pyramid (chosen with an identical area).

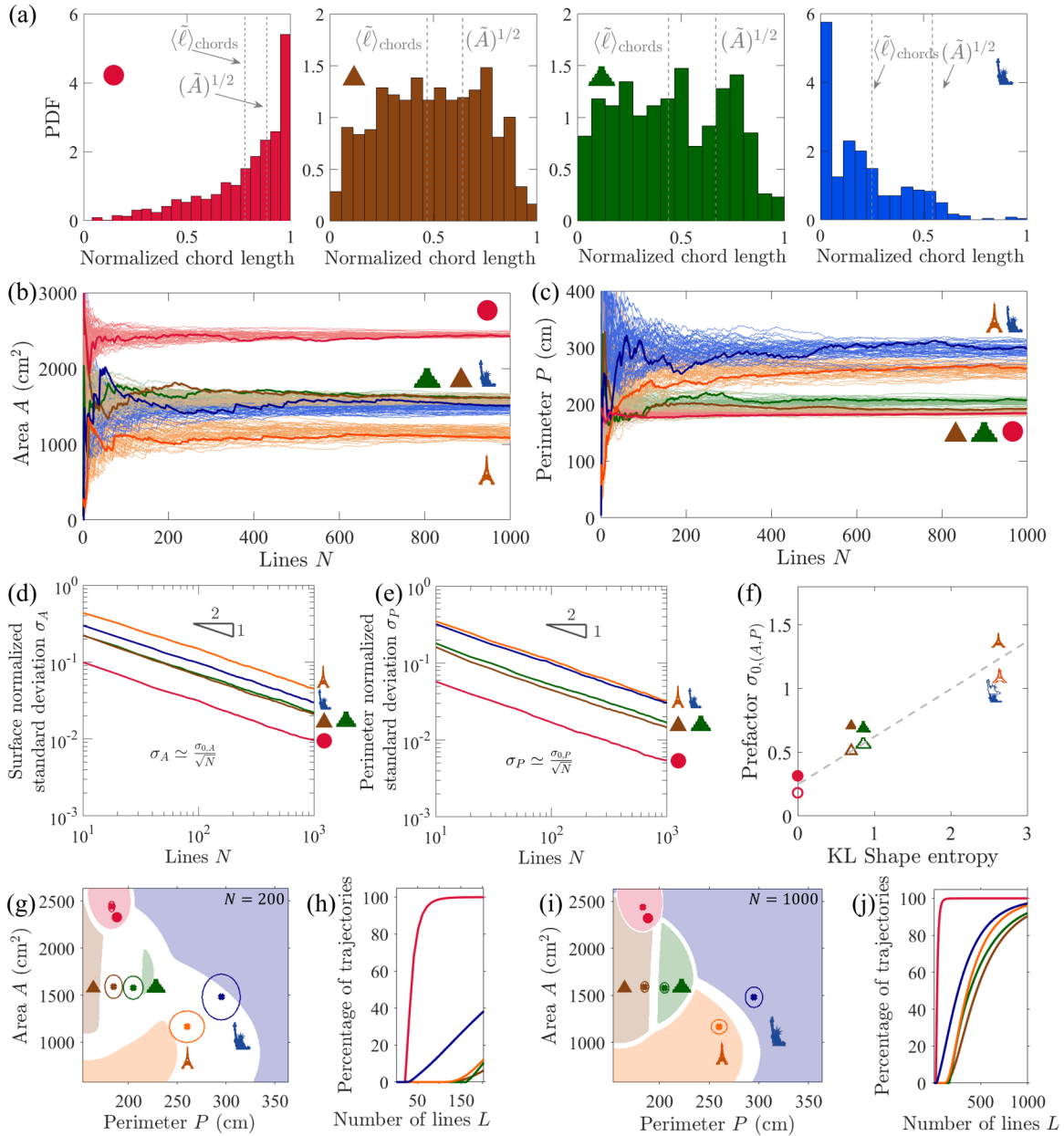


FIG. 3. Convergence properties. Common color code: Circular shape (pink), Chichén Itzá pyramid (green), triangle (brown), Statue of Liberty (blue), Eiffel Tower (orange). (a) Probability density function of chords for the four remaining shapes. The normalized mean chord length invariant $\langle \ell \rangle_{\text{chords}}$ and $\tilde{A}^{1/2} = \left(\frac{\pi}{3} \frac{(\mathcal{L}_3)_{\text{lines}}}{(\mathcal{L}_1)_{\text{lines}}}\right)^{1/2}$ for comparison. Lengths are normalized by the maximum chord length for each shape and are indicated by a tilde sign. (b),(c) Evolution of the area and perimeter estimated autonomously by the robot during its exploration. Thick lines correspond to an experimental realization, thinner lines correspond to Monte Carlo simulations and give an indication of the reduction of the fluctuations over different realizations. (d),(e) Evolution of the standard deviation of the surface and perimeter computed from 1000 independent Monte Carlo simulations as the function the number of lines and follows a $1/2$ power law convergence $\sigma_A \simeq \sigma_{A,0}/\sqrt{N}$ and $\sigma_P \simeq \sigma_{P,0}/\sqrt{N}$. (f) Evolution of the prefactor $\sigma_{A,0}$ or $\sigma_{P,0}$ with the shape entropy of the domain defined as the Kullback-Leibler divergence (KL) of the chord distribution. The dashed grey line is a guide for the eye. The chord distribution of a circular shape is taken as a reference for the KL calculation. (g),(i) Likelihood landscape in the representation space for $N = 200$ (g) and $N = 1000$ (i). The borders indicate a 95% of likelihood of recognition and strongly depend on the dictionary entries. (h),(j) Relative number of lines contributing to a 95% likelihood of recognition for $N = 200$ (h) and $N = 1000$ (i).

D. Efficiency of the method

The extreme frugality and efficiency of the recognition pathway relies on iterative averaging of the statistical features. Figure 3(a) shows the distributions of the chord lengths normalized by the maximal length associated to various ex-

plored shapes. The full chord length distribution obviously holds some additional geometric information from the shape as shown by distinct profiles. However, in the quest for the simplest exploration strategy, the robot does not need to store all these data. It only iteratively computes and save the mean

values $\langle l \rangle_{\text{chords}}$, $\langle \mathcal{L}_1 \rangle_{\text{lines}}$, and $\langle \mathcal{L}_3 \rangle_{\text{lines}}$. This is performed after each exploration line. Note that even the full knowledge of the chord PDF would not be sufficient to establish a strict correspondence with all possible 2D shapes [32]. For a non-convex shape, a line contains at most \mathcal{N} ingoing and outgoing intersection points ($\mathcal{N} = 1$ for convex shapes). The robot thus needs to temporarily store at most $\mathcal{N}(\mathcal{N} - 1) + 4$ values. For a complex shape such as the Statue of Liberty, $\mathcal{N} \leq 6$ and the robot needs to store at most 34 scalar values. While memory is not restrictive for large robots, it is essential for applications at small scales.

We now investigate the convergence to assess the efficiency of this probabilistic method. Figures 3(b) and 3(c) show the evolution of the surface area A and the perimeter P respectively as a function of the number of lines N . The values are computed by the robot during experiments associated to the five shapes in the shape dictionary (colored contrasted solid lines). The robot is programmed to send these updated geometrical estimates by wireless Bluetooth connection only for control purposes as it performs on-board surface and perimeter estimations. Additionally, we perform Monte Carlo simulations by generating uniformly distributed random lines (colored dimmed solid lines) to compare with the experiments. The convergence towards the expected values of P and A for the experimental and simulated estimates are similar. It is found that only a few hundred lines are typically required to measure the area and perimeter with an error of less than 10%. This is sufficient to distinguish the shapes listed in our dictionary. However, in the general case, the recognition speed would strongly depend on the L_2 norm in the representation space {Perimeter-Area} between shapes listed in the dictionary. The standard deviation over many independent realizations can be computed from the numerical simulations as a function of the number of exploration lines N . Figures 3(d) and 3(e) show the evolution of the standard deviations of A , $\sigma_A(N)$ and of P , $\sigma_P(N)$, respectively for the five shapes of the dictionary. It is found that the convergence, in both cases, is independent of the complexity of the explored shape and scales as $1/\sqrt{N}$. This can be rationalized by noting that the measure converges towards a normal distribution as an ensemble averaging of independent random variables with the same mean and standard deviation. The influence of the shape appears only in the prefactors $\sigma_{0,A}$ and $\sigma_{0,P}$ associated to A and P , respectively. The latter increases from the circle, to the square, to the triangle, to the Chichen Itzá pyramid, to the Eiffel Tower, and finally, to the Statue of Liberty. The prefactors thus seem to increase with the complexity of the shape. For regular shapes, complexity can be related to the decrease of the symmetries. For irregular shapes, complexity needs to be assessed quantitatively. The Kullback-Leibler divergence D_{KL} which is a measure of the relative entropy between two probability distributions provides such a parameter. Figure 3(f) shows the prefactors $\sigma_{0,A}$ and $\sigma_{0,P}$ as a function of the D_{KL} of the chord length distributions associated to the various shapes, with the chord length distributions of a circle taken as a reference. The prefactors increase monotonically with D_{KL} confirming the role of complexity. However, the range is only a factor of about 4 for a logarithmic variation between distributions of about 3. The dependence on shape complexity is therefore rather modest.

In practice, the exploration must be stopped, once the likelihood of determining a shape is larger than a preset value, here 95%. The corresponding likelihood landscape (see Supplemental Material Sec. 2 [31]) in the representation space {Perimeter-Area} depends on the given dictionary, $\sigma_{0,A}$ and $\sigma_{0,P}$ for all of the entries, their relative distance in the {Perimeter-Area} space, and the duration of the exploration. Figures 3(g) and 3(i) illustrate the influence of the number of crossing lines N , where each colored domain delineates a 95% likelihood of finding the targeted shape (for $N = 200$ and 1000). Figures 3(h) and 3(j) show quantitatively the relative number of lines contributing to a 95% likelihood of recognition. One observes that about a hundred lines are enough to recognize a circular shape with this level of certainty which is due to its distance from the other shapes in the representation space {Perimeter-Area}. In contrast, it takes more than 10^3 lines to achieve this level of confidence for the other shapes that are more closely packed in the representation space {Perimeter-Area}.

E. Reading letters and words

Equation (1) remains valid for arbitrary shapes with inclusion or even nonconnected shapes. Disconnected objects can thus be explored and gathered within a common global shape with area or perimeter equal to the sum of those of its parts. Since the area and perimeter are geometrical invariants, they are conserved under rigid body transformation such as translations, rotations, mirrors, and any combinations of them (see Supplemental Material Sec. 3 [31]). Two alternative strategies can be chosen to recognize unconnected shapes: a global strategy considering all the shapes as a single clustered entity, or a local strategy considering the addition of each subentity separately. We assess these two strategies through the emblematic case of reading, based on a word or letter-by-letter recognition strategy. The local strategy consists of mapping the capital alphabetic letters into the {Perimeter-Area} representation space which depends on the font. Figure 4(a) shows the position of the projected capital letters for a Helvetica font and the associated domain where the likelihood of recognition is larger than 95% for $N = 3 \times 10^4$. Most common fonts do not overlap in the dictionary partly because letters do not transform into each other by symmetry. Figure 4(b) specifies the number of lines required to distinguish a given letter with a likelihood larger than 95%. Letters can thus be distinguished without ambiguity. For the global strategy, the dictionary is composed of words in the {Perimeter-Area} representation space. Figure 4(c) shows the dictionary with words sampled from the preamble of the United Nations charter as a dictionary [33] with the associated 95% likelihood domains. All the words can be distinguished. One necessary condition for nonoverlapping in the dictionary is the absence of anagrams. In order to compare with the local strategy [Fig. 4(b)], Fig. 4(d) specifies the number of lines, normalized by the number of letters in the word, required to distinguish a given letter with a probability larger than 95%. For this moderately small pool of words, the two strategies are of about the same efficiency.

Figures 4(e) and 4(f) illustrate the principle of these strategies applied to the word ‘‘FREEDOM’’ with successive

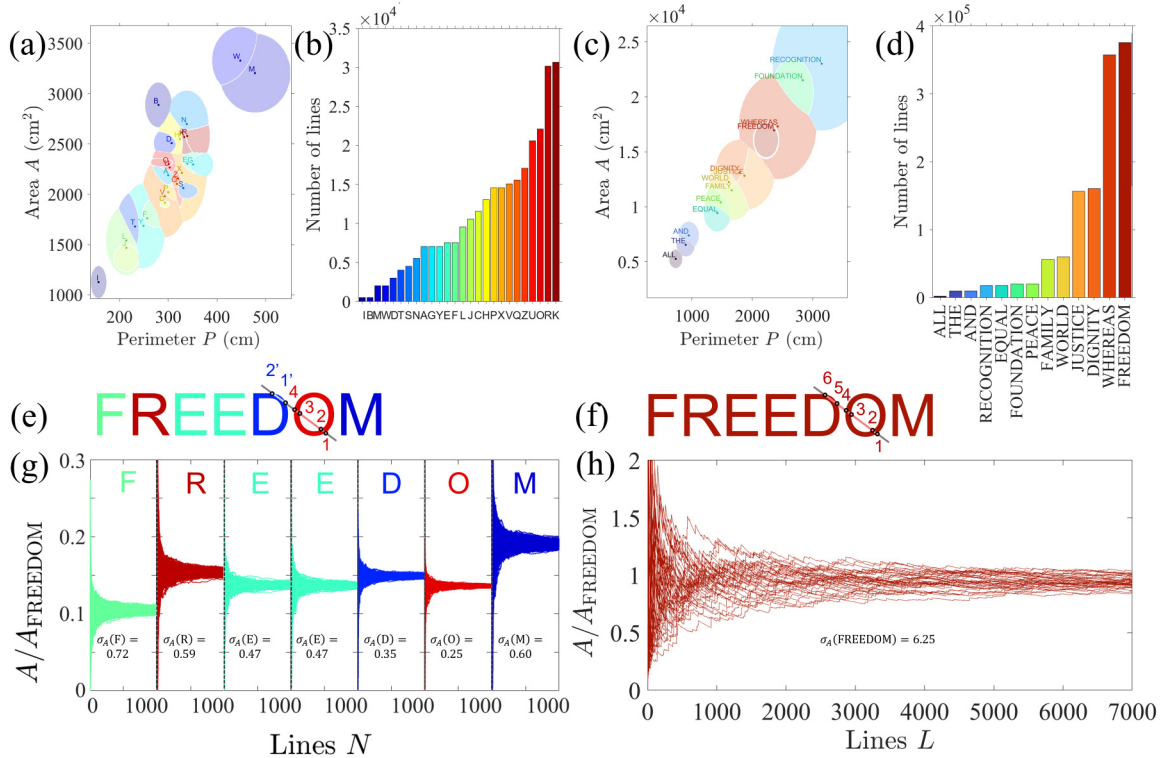


FIG. 4. Global versus local exploration strategies applied to reading. (a) Likelihood landscape in the {Perimeter-Area} representation for the projected capital letters of the alphabet with a likelihood larger than 95%. (b) Specifies the number of lines required to distinguish a given letter without ambiguity, in this case with more than 95% of probability. (c),(d) Global strategy. The dictionary is composed of words in the {Perimeter-Area} representation space. (c) Words sampled from the preamble of the United Nations charter as a dictionary [33] with the associated 95% likelihood domains. The words can be distinguished if there is an absence of anagrams. (d) Number of lines, normalized by the of letter in the word, required to distinguish a given letter with a probability larger than 95%. (e),(f) Comparison of both strategies applied to the word “FREEDOM” with successive identification of each letter (e) and the global estimate (f) of the word perimeter and area. (g),(h) Area estimation of the word FREEDOM and its associated error, with a local (g) or a global (h) strategy. With this moderately small pool of words, the two strategies are of about the same precision.

identification of each letter [Fig. 4(e)] and the global estimate [Fig. 4(f)] of the word perimeter and area. In Figs. 4(g) and 4(h), we plot the convergence for the area estimation in the case of a letter-by-letter strategy or a global strategy, respectively. With this moderately small pool of words, the two strategies are of about the same precision.

The best strategy is a compromise between the size, the choice of the word dictionary, and the accumulation of independent errors in the letter-by-letter strategy. On one hand, if the word dictionary is larger than our current one, the words accumulate in a closed region of the Perimeter-Surface space, and as a consequence, a letter-by-letter strategy is more efficient. On the other hand, if we choose a letter-by-letter strategy, the perimeter and surface area computation accumulate the uncertainties corresponding to each letter. In contrast, the direct word recognition combines the chords topology such that the overall noise is smaller. So, for smaller pool of words, measuring directly the word FREEDOM converged quickly by a “word” rather than a letter-by-letter recognition.

III. CONCLUSION

The strategy, presented here, does not require any knowledge about either absolute or relative position or information

about the direction of motion. On the contrary, the randomness of orientation and absolute position is crucial. At every single stage of the physical computing, the robots acquire no global information about the number of holes, the convexity, or any global information. However, despite ignoring about any global information and by measuring only local quantities, the robot is able to recognize shapes listed in a dictionary by measuring the perimeter and the area of any given 2D shapes. This was only possible thanks to the introduction of a generalized statistical invariant which allows us to estimate the area from a random exploration of any 2D domain, regardless of its complexity. Finally, we note that the dictionary is not a necessary prerequisite and is used here for convenience. A preclassification phase, for example with *k*-means or Gaussian mixture strategies, can be added to our protocol to perform an autonomous and unsupervised recognition. Extending our technique to a swarm of robots, to take advantage of distributive computation strategies, is a natural step where each can compute these invariants locally and share them with the others to improve convergence. However, the inevitable contact between individuals and the possible formation of aggregates makes swarm computation a real challenge, for which new invariants for more disordered paths need to be discovered.

All data are available in the main text or the Supplemental Material [31].

ACKNOWLEDGMENTS

We acknowledge funding from European Union's Horizon 2020 (Marie Skłodowska-Curie Grant No. 754387), AXA Research Fund, CONACYT Mexico (Mobility Grant No. CVU-849369), and the French National Research Agency (Grant No. ANR-10-LABX-24).

E.F. and M.L. contributed the conceptualization, S.H.C., A.C., E.F., and M.L. contributed the methodology, the investigation was carried out by S.H.C., A.C., E.F., and M.L., the visualization by M.L., E.F., and S.H.C., the funding acquisition by M.L., the project administration by M.L. and E.F., supervision by M.L. and E.F., writing the original draft by M.L. and E.F., and writing, reviewing, and editing by M.L., E.F., S.H.C., and A.C.

Authors declare that they have no competing interests.

-
- [1] M. Rubenstein, A. Cornejo, and R. Nagpal, Programmable self-assembly in a thousand-robot swarm, *Science* **345**, 795 (2014).
- [2] M. Y. Ben Zion, J. Fersula, N. Bredeche, and O. Dauchot, Morphological computation and decentralized learning in a swarm of sterically interacting robots, *Sci. Rob.* **8**, eabo6140 (2023).
- [3] G. McIntyre, Estimation of plant density using line transects, *J. Ecol.* **41**, 319 (1953).
- [4] R. Jeanson *et al.*, Self-organized aggregation in cockroaches, *Anim. Behav.* **69**, 169 (2005).
- [5] S. Weitz, S. Blanco, R. Fournier, J. Gautrais, C. Jost, and G. Theraulaz, Residence times and boundary-following behavior in animals, *Phys. Rev. E* **89**, 052715 (2014).
- [6] G. Frangipane *et al.*, Invariance properties of bacterial random walks in complex structures, *Nat. Commun.* **10**, 2442 (2019).
- [7] G. Matheron and J. Serra, *Image Analysis and Mathematical Morphology* (Academic, London, 1982).
- [8] A. Mazzolo, Probability density distribution of random line segments inside a convex body: Application to random media, *J. Math. Phys.* **44**, 853 (2003).
- [9] E. E. Underwood, *Quantitative Stereology*, 2nd ed. (Addison-Wesley, Reading, MA, 1970).
- [10] T. B. Borak, A method for computing random chord length distributions in geometrical objects, *Radiat. Res.* **137**, 346 (1994).
- [11] S. Torquato, *Random Heterogeneous Materials: Microstructure and Macroscopic Properties* (Springer-Verlag, New York, 2002).
- [12] P. Dirac, Approximate rate of neutron multiplication for a solid of arbitrary shape and uniform density, Declassified British Report MS-D-5, Part I, 1943.
- [13] K. M. Case, *Introduction to the Theory of Neutron Diffusion*, (Los Alamos Scientific Laboratory, Los Alamos, NM, 1953).
- [14] W. J. M. de Kruijf and J. L. Kloosterman, On the average chord length in reactor physics, *Ann. Nucl. Energy* **30**, 549 (2003).
- [15] A. Mazzolo, B. Roesslinger, and C. M. Diop, On the properties of the chord length distribution, from integral geometry to reactor physics, *Ann. Nucl. Energy* **30**, 1391 (2003).
- [16] A. L. B. Cauchy, *Mémoire sur la Rectification des Courbes et la Quadrature des Surfaces Courbes* (Gauthier-Villars, Paris, 1832).
- [17] L. A. Santaló, *Integral Geometry and Geometric Probability* (Cambridge University Press, Cambridge, 2004).
- [18] S. Blanco and R. Fournier, An invariance property of diffusive random walks, *Europhysics Lett.* **61**, 168 (2003).
- [19] A. Mazzolo, Properties of uniform random walks in bounded convex bodies, *J. Phys. A: Math. Gen.* **37**, 7095 (2004).
- [20] O. Bénichou, M. Coppey, M. Moreau, P. Suet, and R. Voituriez, Averaged residence times of stochastic motions in bounded domains, *Europhys. Lett.* **70**, 42 (2005).
- [21] A. Mazzolo, On the generalization of the average chord length, *Ann. Nucl. Energy* **35**, 503 (2008).
- [22] A. Mazzolo, C. de Mulatier, and A. Zoia, Cauchy's formulas for random walks in bounded domains, *J. Math. Phys.* **55**, 083308 (2014).
- [23] P. Shukla and D. Thongjaomayum, Surprising variants of Cauchy's formula for mean chord length, *Phys. Rev. E* **100**, 050103(R) (2019).
- [24] A. Mazzolo, Invariance properties of random curves: An approach based on integral geometry, [arXiv:2011.06343](https://arxiv.org/abs/2011.06343).
- [25] S. Hidalgo-Caballero, A. Cassinelli, M. Labousse, and E. Fort, Mean arc theorem for exploring domains with randomly distributed arbitrary closed trajectories, *Eur. Phys. J. Plus* **137**, 1 (2022).
- [26] J. Bardsley and A. Dubi, The average transport path length in scattering media, *SIAM J. Appl. Math.* **40**, 71 (1981).
- [27] R. Pierrat, P. Ambichl, S. Gigan, A. Haber, R. Carminati, and S. Rotter, Invariance property of wave scattering through disordered media, *Proc. Natl. Acad. Sci. USA* **111**, 17765 (2014).
- [28] R. Savo, R. Pierrat, U. Najar, R. Carminati, S. Rotter, and S. Gigan, Observation of mean path length invariance in light-scattering media, *Science* **358**, 765 (2017).
- [29] A. Mazzolo, B. Roesslinger, and W. Gille, Properties of chord length distributions of nonconvex bodies, *J. Math. Phys.* **44**, 6195 (2003).
- [30] <https://sphero.com/collections/coding-robots>.
- [31] See Supplemental Material at <http://link.aps.org/supplemental/10.1103/PhysRevResearch.6.023103> for Movie 1 illustrating the robot exploration; Movie 2 showing an example of convergence in the representation space; the experimental dimensions of the projected shapes; the computation of the likelihood map; the invariance of the method with respect to local rigid transformations.
- [32] C. L. Mallows and J. M. C. Clark, Linear-intercept distributions do not characterize plane sets, *J. Appl. Probab.* **7**, 240 (1970).
- [33] U. N. G. Assembly, *Universal Declaration of Human Rights* (Department of State, Washington DC, 1949), Vol. 3381.